Recent Developments in the Design of Photoactivated Metal Oxide Gas Sensors and Application of Plasmonic Nanoparticles in Hydrogen-Sensing Devices

Ingo Weyrauch,* Eva Louisa Hefler, Rene Breuch, Peter Kaul, Sanjay Mathur, and Kostyantin Konstantynovski

Recent advancements in photoactivated metal oxide (MOX) gas sensors and the application of plasmonic nanoparticles (NPs) in hydrogen sensing have demonstrated significant potential in enhancing sensor performance. Hydrogen, as a high-energy, carbon-free alternative to fossil fuels, requires reliable detection methods due to its storage and handling risks. Traditional MOX gas sensors, while cost-effective and versatile, face challenges such as high operating temperatures and limited selectivity. In this review, innovative photonic methods are explored to overcome these limitations, focusing on photoactivation and plasmonic effects. Photonic activation improves sensitivity, response time, and recovery time at room temperature, mitigating the safety risks associated with high-temperature operations. Additionally, the integration of plasmonic NPs, made from gold, palladium, or other less noble metals, into MOX gas sensors enhances catalytic activity and sensor response through localized surface plasmon resonance. In this review, also the synergistic effects of noble metal decoration and photonic enhancement are covered, providing a comprehensive overview of the current state and possible future directions in hydrogen-sensing technology. These advancements promise safer and more efficient hydrogen detection, crucial for the expanding hydrogen infrastructure and its role in a sustainable energy future.

I. Weyrauch, E. L. Hefler, R. Breuch, P. Kaul, K. Konstantynovski
German Aerospace Center (DLR)
Institute for the Protection of Terrestrial Infrastructures
Rathausallee 12, 53757 Sankt Augustin, Germany
E-mail: ingo.weyrauch@dlr.de

I. Weyrauch, P. Kaul
Institute for Safety and Security Research
University of Applied Sciences (H-BRS)
Von Liebig-Straße 20, 53359 Rheinbach, Germany

S. Mathur
Institute of Inorganic Chemistry
University of Cologne
Greinstraße 6, 50939 Cologne, Germany

1. Introduction

Hydrogen as an energy carrier has become one of the most promising candidates to provide sufficient energy for an expanding world population, while serving as a carbon-free alternative to fossil fuels. Compared to gasoline, hydrogen gas has a three times higher energy content per mass and is applicable in many sectors of economy, like transport, energy, and chemical industries.[1] Therefore, an increasing production, storage, and application are inevitable. In their Net Zero Emissions by 2050 Scenario, the International Energy Agency IEA predicts an international hydrogen demand of over 200 Mt in 2030.[2] This would be an increase of more than 100% compared to 2020, showing the importance of expanding the existing hydrogen infrastructure in the near future. Since hydrogen is commonly stored under high pressures and has the potential to form explosive mixtures in air at concentrations between 4% and 77%, a high safety risk is related to the storage, transport, and usage of hydrogen.[3,4] Consequently, a fast and reliable detection of hydrogen gas leakages is critical for the safety and public acceptance for this energy carrier. In addition to the explosion risk, hydrogen gas is highly reactive as a reducing agent. Therefore, the development of reliable detection methods to monitor even small concentrations is a critical task for the industry. The U.S. Department of Energy (DOE) has specified targets for the development of hydrogen safety sensors: these include a measuring range of 0.1–10%, operating temperatures from −30 to 80 °C, response times below 1 s and resistance against interferences (e.g., hydrocarbons) in ambient air with 10–98% relative humidity (RH).[5] This review aims to give an overview of the recent developments in metal oxide (MOX) sensor design and an evaluation to the state of completion of the DOE requirements.

One group of gas sensors that has been intensively studied over the past decades is semiconductor gas sensors made from various MOX semiconductors. The first report on their measuring principle was published in 1954 by Heiland, who investigated the influence of hydrogen and oxygen on the electrical resistance of ZnO.[6] Later on, Seiyama et al. reported on the first ZnO

ADVANCED
SCIENCE NEWS

www.advancedsciencenews.com

physica
status
solidi a

www.pss-a.com

sensor for the detection of hydrogen and alkanes.[7] In general, transition MOXs with d_0 or d_{10} configuration are viable candidates for gas-sensing applications[8,9] but n-type semiconductors like SnO_2, WO_3, ZnO, and TiO_2 are among the most intensively studied materials for MOX gas sensors.[10] MOXs, like SnO_2 und TiO_2, are wide-bandgap materials, restricting the transition of electrons from the valence to the conduction band, lowering the conductivity.[11] Contrary, defects at the surface of crystal lattice, such as oxygen vacancies, leave energetic electrons behind, giving the material n-type characteristics and decreasing the electrical resistance.[11] Further chemisorption of oxygen from ambient air by the uptake of electrons from the semiconductor leads to various surface states of oxygen ions and energy band bending at the surface of the semiconductor.[12] The depletion of charge carriers and the depletion depth can alter the conductivity of the sensing element significantly and are the base for the reaction and transduction principle of resistive semiconductor gas sensors. Adsorption of different gas species on the semiconductor and their interactions with surface states of oxygen leads to partial-pressure-dependent resistances of the sensing layer.[12] Chemisorption of oxygen is limited by two factors: chemically, due to the activation energy for adsorption and desorption processes, and electrically as the increasing charge on the surface creates a potential barrier that electrons have to overcome for further adsorption.[13] Consequently, the coverage of oxygen on the semiconductor surface is determined by the oxygen partial pressure, adsorption and desorption kinetics connected to the temperature, as well as the ionization state of oxygen. When atmospheric oxygen O_2 is adsorbed at the surface of a semiconductor, depending on the temperature, different oxygen species can form.[13,14] At temperatures below 150 °C, molecular chemisorbed O_2^- predominates while above this temperature atomic ionic species O^- and O^{2-} will form.

$$O_{2(gas)} + e^- \rightarrow O_{2(ads)}^- \quad (1)$$

$$O_{2(ads)}^- + e^- \rightarrow 2O_{(ads)}^- \quad (2)$$

$$O_{(ads)}^- + e^- \rightarrow O_{(ads)}^{2-} \quad (3)$$

The conductivity of the sensing layer is further influenced by redox reactions of gases with the adsorbed oxygen species or the semiconductor itself. In case of hydrogen as a reducing agent, adsorbed oxygen species can react with the analyte to form water and release electrons back into the conduction band of the semiconductor.[14–16]

$$2H_{2(gas)} + O_{2(ads)}^- \rightarrow 2H_2O + e^- \quad (4)$$

$$H_{2(gas)} + O_{(ads)}^- \rightarrow H_2O + e^- \quad (5)$$

$$H_{2(gas)} + O_{(ads)}^{2-} \rightarrow H_2O + 2e^- \quad (6)$$
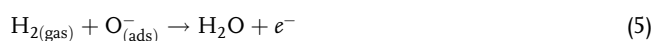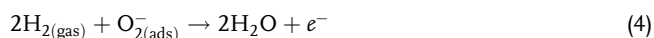
From the reactions (Equation (4)–(6)), it can be concluded that oxygen species with lower oxidation numbers will reintroduce more electrons back in the semiconductor upon reaction with a reducing gas and would therefore show a more pronounced change in signal. In addition to elevated adsorption kinetics, this

is one of the reasons why MOX gas sensors are commonly operated at elevated temperatures >150 °C.[16]

For p-type semiconductors such as NiO, CuO, and Co_3O_4,[17,18] charge transfer does not occur via electrons but positively charged holes resulting from defects, for example, metal vacancies or interstitial impurities, in the crystal lattice.[19,20] Consequently, upon contact with oxygen, the uptake of electrons from a p-type semiconductor leads to an increased number of holes, improving the electrical conductivity of the material. **Figure 1** shows the reaction of n-type and p-type MOX gas sensors upon contact with reducing gases. Since reducing gases can reintroduce electrons in the material, the resistance of a n-type semiconductor decreases upon gas contact, while p-type semiconductors react in the opposite way.

Typical MOX-sensor surfaces are composed of sintered crystallites or grains that are connected by grain boundaries. As already mentioned, adsorbed oxygen extracts electrons from the grain surface resulting in a charge depletion zone called the space-charge layer with high electrical resistance[21] shown in **Figure 2**. The ratio of crystallite diameter D and the width of the space-charge region have a significant influence on the sensitivity of the sensor. When the size of the grain increases, the depletion area extends less deep into the grain, altering the transducing behavior of the MOX layer.

According to Xu et al. three different scenarios can be distinguished,[22] as shown in **Figure 3**: When D » 2L, the influence of surface reactions on the overall conductivity is minor, as electron conduction can occur via the bulk region (grain boundary control). The sensitivity increases when D is close to 2L, as necks of the interconnected grains become the most resistant and mainly determine the conductivity of the sensing layer (neck control). For crystallite diameters smaller than 2L, the space-charge region extends over the entire grain. As a result of the fully depleted grains, resistance drastically increases leading to improved sensitivity of the sensor. This so-called flat-band condition, where no bending of the energy bands occurs, is highly favorable for efficient sensor designs and explains why nanomaterials find vast application in sensor development.[13]
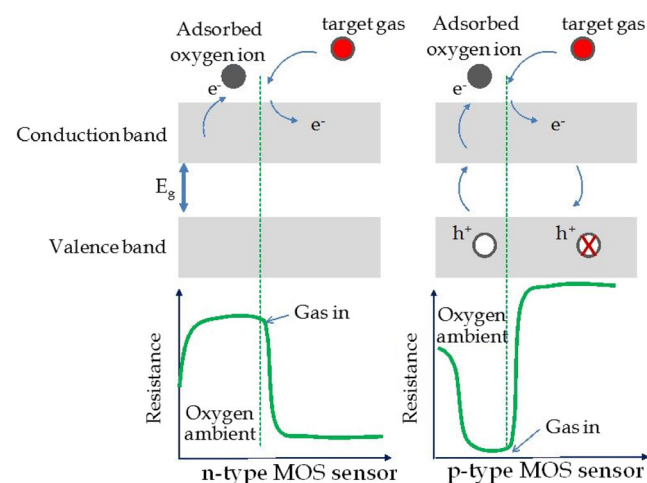
Figure 1. Reaction and resistance change of n-type and p-type semiconductors upon contact to a reducing gas. Reproduced under terms of the CC-BY license.[19] Copyright 2012, published by IntechOpen.
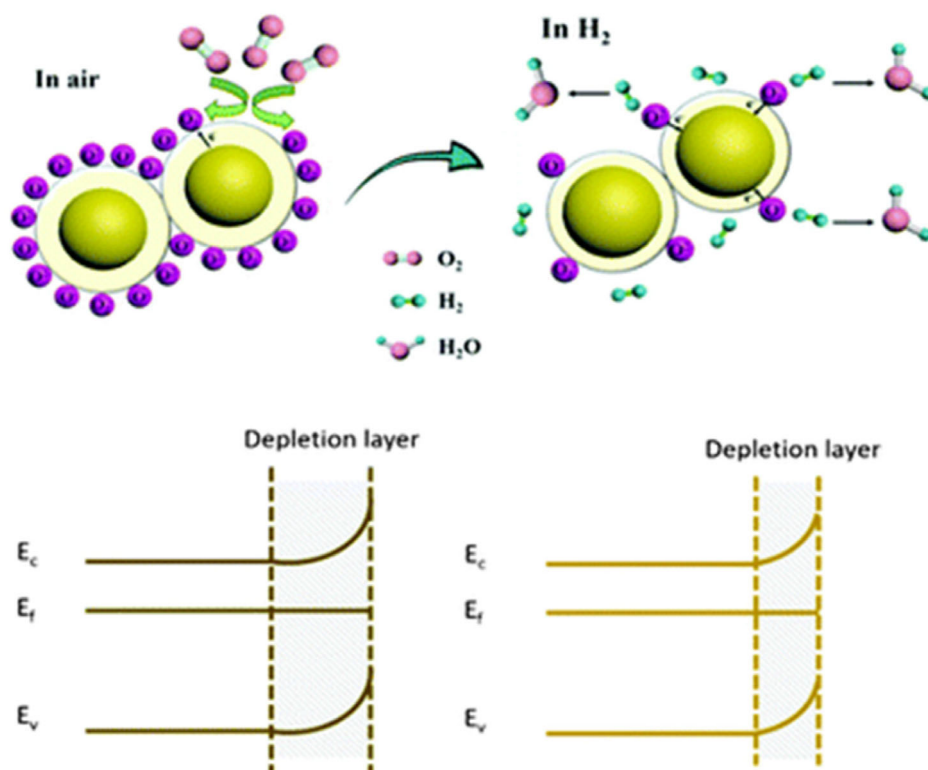
Figure 2. Interaction and formation of a depletion layer of a n-type semiconductor upon contact to atmospheric oxygen and hydrogen gas. E_c refers to the energy of the conduction band, E_v to the energy of the valence band and E_f to the corresponding fermi energy. Reproduced with permission[14] Copyright 2021, published by the Royal Society of Chemistry.

MOX gas sensors find wide application in the industry due to their excellent sensing performance, low production costs, small size, and the high variety of gases that can be measured.[23] Especially the low costs and size are a big advantage of this kind of sensors compared to other suitable detection methods, such as infrared (IR) spectroscopy and gas chromatography/mass spectrometry combinations.[24] Nevertheless, there are still challenges associated with the fabrication and use of MOX gas sensors for the detection of hydrogen, such as low selectivity, insufficient long-term stability of thin films, and relatively slow reaction and recovery times at low temperatures.[24] Accelerated surface reactions and their intrinsically low electrical conductivity is another reason why MOX gas sensors are usually operated at elevated temperatures >300 °C, increasing the costs and the energy consumption and more importantly creating an additional safety risk for their operation in hydrogen-rich atmospheres.[5] A number of concepts have been put forward to lower the operating temperatures as well as increasing the sensitivity and selectivity by loading the MOX gas sensor surface with catalytic noble metals,[25–29] utilizing nanostructures with enhanced surface reaction properties,[29–34] or creating metal–MOX heterostructures.[33,35,36] To achieve maximum performance, attempts have been made to even combine several approaches; however, selective sensing of hydrogen at room temperature (RT) remains a challenge. A less frequently discussed pathway of sensor optimization is the activation of MOXs with photonic irradiation and the application of new achievements from photocatalysis. This review article summarizes the recent developments in photonic methods to enhance the performance of semiconductor gas sensors with special attention to optical surface effects, such as laser desorption, photoactivation, and surface plasmon resonance.

2. Light-Induced Surface Effects

The application of light-induced surface effects offers several opportunities to overcome the challenges associated with semiconductor gas sensors and improve their performance in general.[37–39] In 2020, Wang et al. reviewed the recent development status of light-activated semiconductor gas sensing.[39] They concluded that the use of photonic irradiation is one of the most effective approaches for optimizing RT gas sensing. The performance indicators considered for this conclusion are significantly improved sensitivity, shortened response and recovery time, reversibility, and humidity resistance of the sensing system. Response and recovery times of a semiconductor gas sensor strongly depend on adsorption and desorption rates of surrounding gas species on the active sensor surface, as well as the amount of free adsorption sites that can be occupied by analyte molecules.[40] Another key factor influencing response times and sensitivity is the diffusion of gas species through the sensitive layer. Surface reactions decrease the availability of gas species, resulting concentration gradient with increasing layer depth.[41] Diffusion through porous materials is influenced by layer
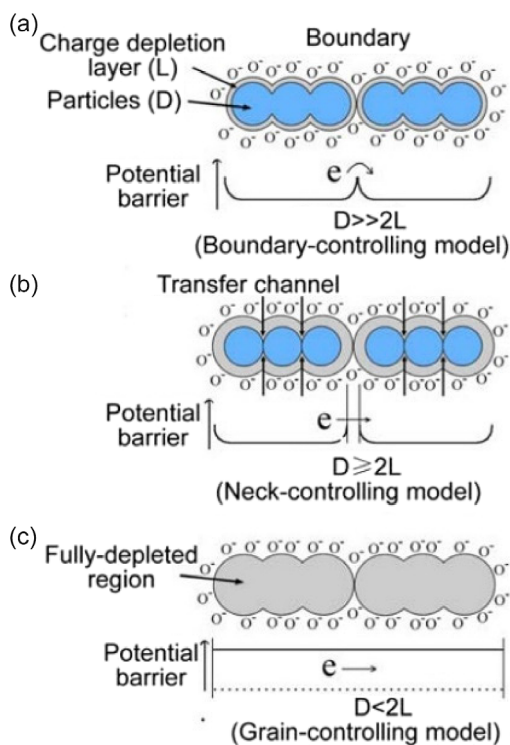
Figure 3. a) Schematic model of the three different scenarios boundary controlling-model, b) neck-controlling model, and c) for charge transfer through interconnected grains of a semiconductor, depending on aspect ratio of crystallite diameter D and the depth of the space-charge region L. Reproduced under terms of the CC-BY license.[21] Copyright 2012, published by MDPI.

thickness, porosity, temperature, and the diffusing gas species.[42] Therefore, most semiconductor gas sensors show effective sensing behavior at elevated operating temperatures, where conductance of the semiconductor and diffusion processes of gas molecules are highly elevated. Since hydrogen can form explosive mixtures in air at a concentrations of above 4%, operating high-temperature MOX gas sensors in hydrogen-rich atmospheres, for example, in case of leakage detection on hydrogen storages or pipelines in enclosed areas, would therefore pose an additional safety risk.[3] Photonic activation of the sensor surface, without the need for thermal energy, might be a suitable attempt to eliminate those issues and ensure safety of hydrogen infrastructures. Already in 1994, Saura investigated the influence of broadband UV irradiation on the gas-sensing properties of SnO$_2$ films.[43] Despite being operated at RTs, the sensors showed fast response toward acetone and trichloroethylene, showing the applicability of light activation to MOX gas sensors. The following text reviews the photoactivation and photodesorption processes on pristine and noble metal-doped MOX gas sensors as well as the current state of hydrogen sensors utilizing those effects.

2.1. Photoactivation and Photodesorption Processes

When the energy delivered by photons illuminating the surface of an MOX gas sensor is greater than the bandgap of the material, free electrons are transferred from the valence to the conduction band.[44] For common MOXs, such as TiO$_2$, SnO$_2$, and ZnO, highest photogenerated carrier densities were achieved by irradiating the materials with UV photons, corresponding to their bandgap energies.[45] SnO$_2$ has a relatively wide bandgap with an energy of 3.5 eV,[45] while TiO$_2$ has a slightly lower bandgap of 3.02 eV for rutile and 3.2 eV for anatase.[46] The gas-sensing mechanism for H$_2$ on polycrystalline ZnO under UV illumination was investigated by Fan et al.[47] From their results they concluded, photoelectrons and photoinduced holes are generated by the illumination of the sensor, these photoelectrons can induce ionization of oxygen in the atmosphere to form weakly bound oxygen ions ($O_2^-(h\nu)$). Contrary, stronger bound chemisorbed O_2^- species with higher desorption energy can interact with the photoinduced electron holes to form O_2 in an equilibrium reaction between adsorption and desorption processes. Upon interacting with reducing gases such as H$_2$, the weakly bound oxygen ions ($O_2^-(h\nu)$) can readily react with the hydrogen molecules to form water, hence reintroducing electrons into the sensitive layer resulting in a more sensitive signal. In the context of this article, it has to be mentioned that O_2^- ions carry a free valence electron.[47] Therefore, the O_2^- ion is more precisely is a radical ion, also called superoxide ion.[48] A slightly different mechanism for photocatalysis on MOXs was proposed by Bodzek and Rajca, who investigated the redox reactions on photoactivated TiO$_2$.[44] They agree that absorbed photons with sufficient energy promote valence band electrons in the conduction band. The electrons in the conduction band then subsequently react with atmospheric oxygen, forming reactive superoxide radicals O_2^-. The difference in their assumptions is that recombination of electron–hole pairs also leads to formation of peroxide radicals by oxidation of atmospheric water, acting as another reactive species for further surface redox reactions. Reddeppa et al. also found a humidity dependence of the sensor signal under illumination, yet no linear behavior of RH and sensor sensitivity could be observed.[49] Though the exact hydrogen-sensing mechanism is complex and still under scope of research, light activation has proven to be an effective alternative for electrical/resistive heating.[39,50]

Photoactivation not only affects the sensitivity of an MOX gas sensor but can also influence selectivity, related to the extent of response to different gas species under similar conditions. Activating different ZnO nanostructures with UV light, Alenezi et al. observed intensity-dependent sensitivity maxima for ethanol, isopropanol, acetone, and toluene.[16] Investigating the enhancement of sensitivity of SnO$_2$ films toward trichloroethylene and acetone by light activation, Saura found that selectivity could be enhanced by altering the excitation spectrum of the light source.[43] This could be utilized in virtual sensor arrays where a single sensor produces multiple signals for a gas species depending on the irradiation conditions, as already proposed by Njio and Wagner.[51] As shown in **Figure 4**, in addition to photocatalysis of surface redox reactions, photodesorption of adsorbed gas species is another photoinduced effect, highly beneficial for fast sensor recovery, especially when operating at RT. Qomaruddin et al. could show that stimulation of their p-type CaFe$_2$O$_4$ with visible light lead to a faster, though not full recovery of the sensor from ethanol as their target analyte.[52] Zhang et al. recently fabricated a NO$_2$ sensor based on In$_2$O$_3$ nanowires (NWs). Without
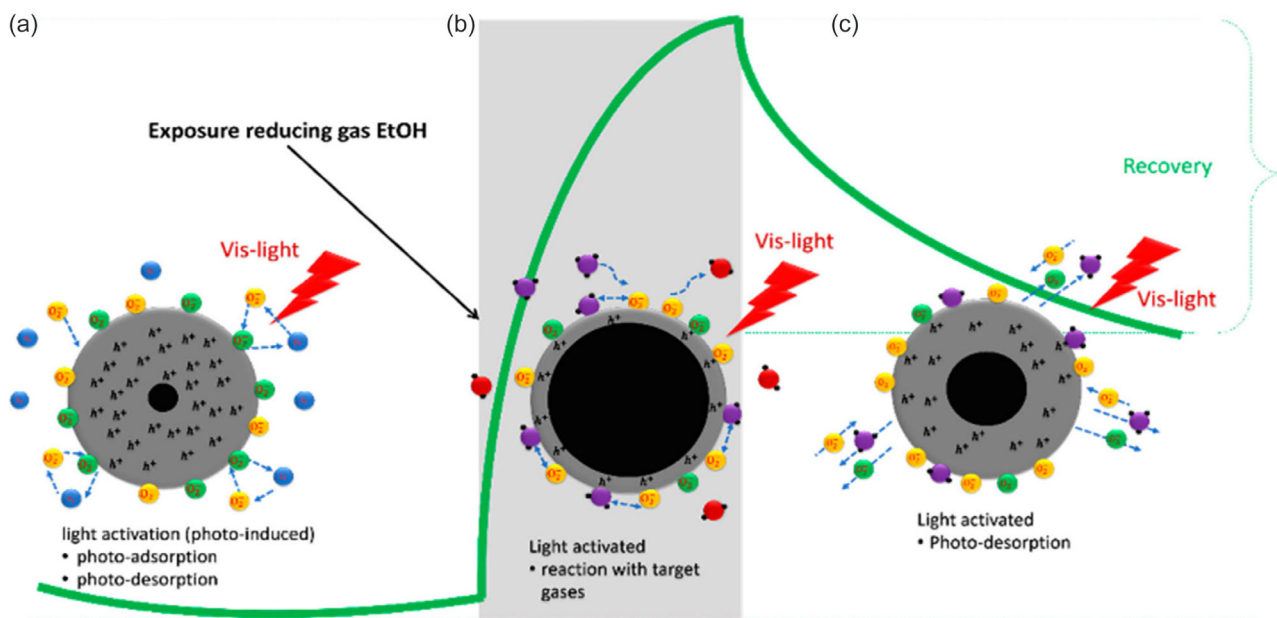
Figure 4. Different effects of photoactivation on the different stages of sensor reaction: a) photoactivation before gas exposure; b) interaction of the target gas with photoinduced reactive oxygen species; and c) enhanced recovery by photodesorption of the reaction product; Reproduced under terms of the CC-BY license.[52] Copyright 2020, published by MDPI.

illumination the sensor took 1000 s to reach 90% of its original resistance after contact to 5 ppm NO_2.[53] Illuminating the sensor with white light in the range of 400–600 nm, 100% recovery could be achieved after only 6 s. They assumed that photogenerated electron holes could not only interact with adsorbed O_2^- but also oxidize NO_2^- species to facilitate their desorption in form of NO_2(g). It was also shown that increasing the light intensity drastically lowered recovery times of the sensor, yet reaction times below 1 s, as required by the DOE, could not be achieved. Concerning operating temperatures of hydrogen safety sensors, vast progress has been made to reduce them to RT.

Though most of them utilize noble metals as catalytic materials to further enhance the sensor performance, also pristine MOXs, which exhibit photocatalytic behavior, are sufficiently investigated. Sihar et al. synthesized CuO NWs by thermal oxidation method.[54] The final sensitive layer was composed of CuO NWs and a Cu_2O thin film deposited on Pt/Cr electrodes as shown in **Figure 5**. At RT, the response of the sensor increased more than tenfold with exposure to 3 mW cm^{-2} UV irradiation at 365 nm. Also, stabilization of the sensor signal took place faster and to a higher extent, if compared to dark conditions.

Park et al. synthesized ZnO–core/WO_3–shell NWs by thermal evaporation of a mixture of ZnO and graphite powders, followed by sputtering of WO_3.[55] At 1000 ppm hydrogen concentration and illumination at 365 nm but only 1.2 mW cm^{-2}, the sensor response was increased more than fivefold compared to measurements without irradiation. Similar results were obtained by Li et al. on nanoconical SnO_2 structures, synthesized by a hydrothermal approach.[56] At an operating temperature of 50 °C and upon exposure to 100 ppm of H_2, sensitivity increased by a factor of 3.5 during illumination with an light emitting diode (LED) array light source at 313 nm with 4 mW cm^{-2}. A rather unusual,

yet highly ecological sensor design was proposed by Saravanan et al. that utilizes biowaste from silk worm cocoons to produce granular-activated carbon (GAC) materials.[57] Coating ZnO nanorods with GAC, they obtained core–shell structures with superior hydrogen-sensing properties, when compared to the pristine ZnO nanorods as a reference. Additionally, the performance improvement by irradiation with UV light was shown to be more efficient on the GAC-coated nanorods. With their sensor design, they achieved relatively short reaction and recovery times of 15 and 18 s.

2.2. Photo-Enhanced Catalysis by Noble Metal Decoration

A significant number of articles and reviews focus on the decoration of nanostructured MOX gas sensors with noble metals, which have shown to effectively lower operating temperatures even without radiation.[58–68] In this context, the creation of Schottky barriers in metal–semiconductor junctions and the hydrogen spillover effect on noble metals play a big role in tuning the sensor performance and will be briefly discussed here, although not being light-dependent effects. Schottky barriers are potential energy barriers for electrons that form at metal–semiconductor junctions, where the barrier height is defined as the difference between the work function of the metal and the electron affinity of the sensor material.[69] Kumar et al. showed that this barrier height has a big influence on the sensitivity of a gas sensor.[70] They fabricated TiO_2 nanoplates by sputtering on a p-Si substrate and contacted the sensing layer with Al, Ni, Au, and Ag as electrode materials. The response of the sensors toward hydrogen was tested in a temperature range of 25–175 °C and showed best results for Au electrodes with the highest Schottky barrier. An explanation for this effect could be that the

ADVANCED
SCIENCE NEWS
www.advancedsciencenews.com

physica
pssa
status
solidi

www.pss-a.com
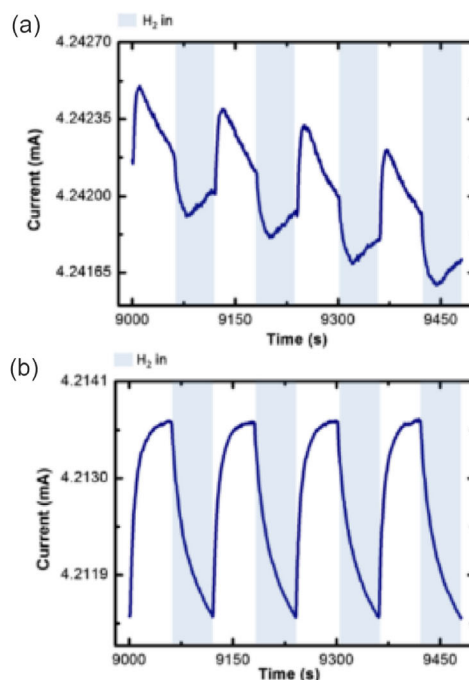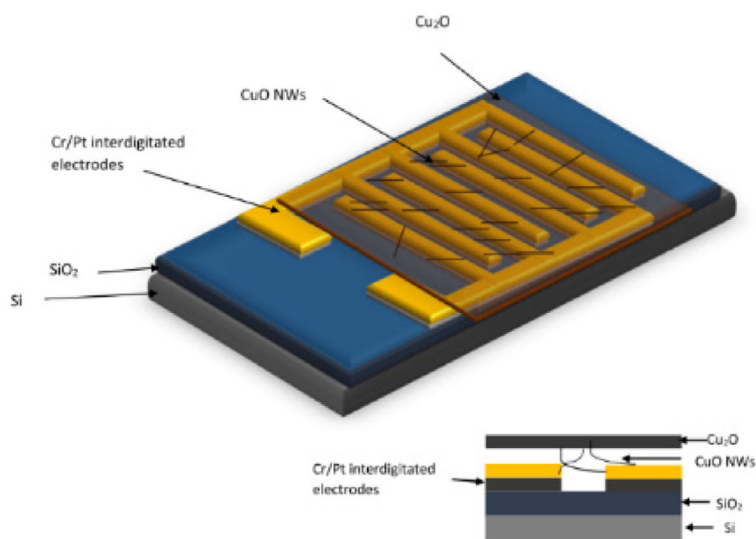
Figure 5. Design of a CuO-nanowire-based MOX gas sensor and its response to hydrogen at room temperature a) should be on the upper graph and b) on the graph below as it demonstrates the influence of light activation on the sensor signal. Reproduced under terms of the CC-BY license.[54] Copyright 2018, published by Springer Nature.

high potential barrier restricts the migration of electrons from the semiconductor to the metal particle, which would reduce the reactivity of the semiconductor. The spillover effect in contrast describes the dissociation and migration of hydrogen atoms from noble metals catalyst to an active support material.[71] This drastically increases the availability of hydrogen on the active material and raises the reactivity of hydrogen due to the dissociation. Though the exact mechanism is still under discussion in the catalysis community, hydrogen spillover is utilized in various catalytic reduction reactions and also hydrogen storage.[72] In addition to those effects, nanostructured materials can lower the activation energy of surface reactions by providing a density of surface states,[63] while noble metals can act as a catalyst in various redox reactions.[64] In 1991, Schierbaum et al. investigated the catalytic activity of Pd deposited on SnO_2 thin films.[73] In addition to the enhanced H_2 conversion due to catalytic activity of Pd, they examined significant temperature-dependent differences in the response for H_2 and CO between Pd-doped and pristine MOX sensors. While H_2 response increased significantly, the CO response decreased with Pd doping. The decrease in response in this case could be explained by poisoning of the catalyst with carbon monoxide, which is known to have a negative influence on the adsorption properties and catalytic activity of palladium.[74] Another major disadvantages of the utilization of precious noble metals are highly increased production costs. A more efficient use of the catalyst could be achieved by light activation of both the sensor material and also the noble metal, though additional costs for light source and electrics have to be considered.[59]

Considering noble metal-doped MOX gas sensors for light activation, a high number of these sensor designs target NO_2 as analyte gas,[53,75–87] while a significantly smaller fraction of research is focused on hydrogen detection.[88–93] Ebtsam et al. fabricated a low-temperature MOX gas sensor based on Pd decorated TiO_2 colloidal crystals.[88] Polystyrene (PS) long-ranged ordered crystals were synthesized via a wet-chemical approach and transferred on a sensor substrate. The surface was then edged with a plasma to reduce particle size and uncover the conductive surface while maintaining a uniform distribution of PS crystals. A thin layer of TiO_2 was then deposited on the PS by chemical vapor deposition and subsequently functionalized with Pd nanoparticles (NPs) by an electroless plating process. The sensor response toward 50–500 ppm of hydrogen was observed at an operation temperature of 33 °C and illuminated by an UV–LED at 365 nm with a power density of 2024 $\mu W\,cm^{-2}$. Their sensor showed superior performance even at this low operating temperature, combining fast response and recovery times of 43 and 24 s, highly increased sensitivity, and a more stable signal under UV irradiation. Considering the selectivity of the sensor, they examined almost no response toward methyl ethyl ketone (C_2H_4O), acetone (C_2H_4O), acetaldehyde (C_2H_4O), nitric oxide (NO), and carbon dioxide (CO_2). Within their experiments, they also investigated the influence of humidity on the sensor signal and found that the sensors response toward 20% RH increased from 0.4% to 7% under irradiation. As a consequence, humidity dependences of the sensor signal might be elevated by irradiation which can be expected to have an even higher influence on the hydrogen-sensing mechanism in which water is created during

the surface reaction with oxygen species.[15] Another light-activated RT hydrogen sensor was presented by Geng et al.[89] WO_3 nanorods were synthesized by a hydrothermal method and functionalized in a $PdCl_2$ solution. After annealing, PdO NPs with a diameter of 20–40 nm found to be adhered to the WO_3 nanorod surface. To evaluate the sensing performance, the resistance of the hybrid material was measured during contact to 40 ppm H_2 while irradiating with different LEDs with light intensity of $0.15\,W\,cm^{-2}$ at wavelengths of 400–600 nm. Compared to a sensor tested under dark conditions and 250 °C operating temperature, they found that the irradiated sensor showed longer response and recovery times of 2.1 and 5.8 min, compared to 1.5 and 3.6 min, while sensitivity on the other side was almost doubled. Additionally, they could show that not only the sensor response but also the response and recovery times are highly dependent on the wavelength of the chosen light source. Irradiation with red LEDs at a wavelength of 640 nm resulted in the highest sensitivity but also highest response and recovery times while choosing shorter wavelengths from a blue LED at 480 nm significantly decreased all of the previous parameters.

As shown in **Figure 6**, Hashtroudi et al. very recently developed a highly sensitive hydrogen gas sensor based on a 2D CeO_2–Pd–polydopamine(PDA)/reduced graphene oxide(rGO) nanocomposite.[90] The nanocomposite was fabricated by a wet chemical approach and drop casted on a 10×6 mm sensor substrate with gold electrodes. Polydopamine was used to reduce and functionalize graphene oxide via self-polymerization. The resistivity of the sensor was measured during gas contact to 50–6000 ppm hydrogen, working temperatures of 30–200 °C, UV irradiation at 365 nm with a power density of $8.9\,\mu W\,cm^{-2}$, and RH up to 30%. The nanocomposite acted as a p-type semiconductor; therefore, the resistivity increases upon exposure to hydrogen. The p-type characteristics of the composite can be explained by the p-type behavior of rGO which has also been observed as a reversible phenomenon in combination with ZnO, where the sensor response could be switched from p-type to n-type by increasing the operating temperature.[94] During illumination, Hashtroudi et al. only observed a small increase in

response but achieved a full recovery of the sensor.[90] In addition to high sensitivity even at RT, long-term stability and selectivity to H_2 could be achieved. In the study, the sensor showed significantly higher response to H_2 (Response = 136%) compared to acetone (C_3H_6O) (Response = 2.6%), nitric dioxide (NO_2) (Response = 38%), ammonia (NH_3) (Response = 1.4%), and methane (CH_4) (Response = 3.2%), where response was defined as the ratio of the sensor resistance with and without the corresponding analyte gas. Since all tested gas species still resulted in a sensor response, identification of the gas species only by the sensor resistance of a single sensor is still impossible. A full overview of the photoactivated hydrogen sensors presented in Section 2 is given in **Table 1**.

The high variation in experimental parameters (operating temperature, humidity, gas concentrations, carrier gas composition, gas chamber design, etc.) as well as inconsistent definitions for sensitivity and response and recovery times make a comparative analysis of these values impractical. This highlights the missing standardization as a key issue for reviewing the publications of different work groups and also identifying the most promising material combinations or optimization routes for further research. The need of qualified data deserves special attention, when AI-based algorithms should be used to predict suitable sensor materials and for the data driven analysis in development of next-generation sensors.

3. Plasmonic NPs

Plasmonic NPs are NPs typically 1–100 nm in size, made from various noble and nonnoble metals, as well as MOXs, metal nitrides, and metal chalcogenides.[95] They possess a broad absorption spectrum from near IR to the UV region,[95,96] which predestines them for excitation by photonic irradiation.[97] Their application in photocatalytic reactions is based on the optical excitation of localized surface plasmon resonance (LSPR),[98] where electrons from the conduction band of a single NP oscillate in resonance of the incident light wave with wavelength comparable to the size of the particle.[97,99] The interaction of the
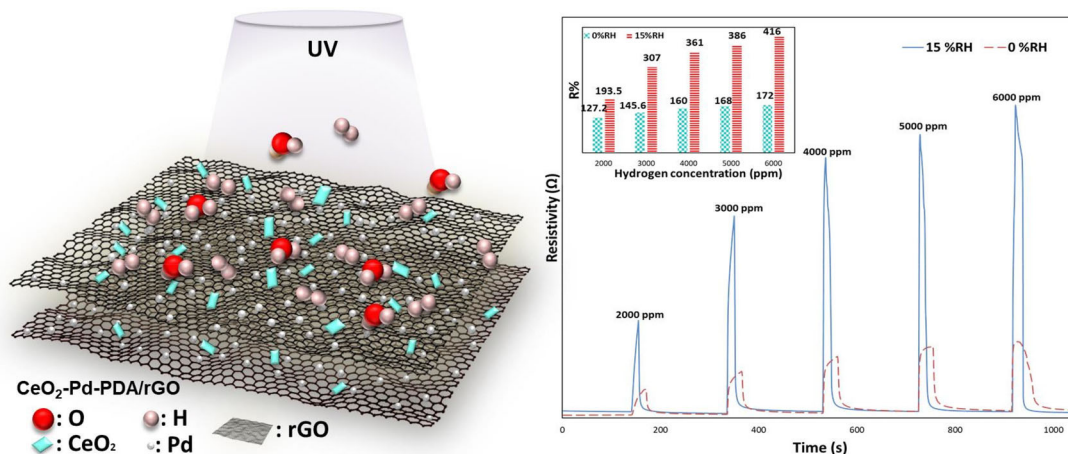
Figure 6. UV-activated CeO_2-Pd-PDA/rGO nanocomposite sensor showing a good response toward hydrogen but a high dependence of the signal on the RH. Reproduced under terms of the CC-BY license.[90] Copyright 2022, published by MDPI.

Table 1. Overview of light-activated hydrogen sensors and their performance parameters reviewed in Section 2.1 and 2.2. Definitions for sensor response (sensitivity) were inconsistent throughout the publications. The response and recovery times correlate to the time needed to achieve 90% of signal change during gas contact or recovery. For fields with "–" no data was available.

Material	Light source	T [°C]	RH [%]	$c(H_2)$ [ppm]	t_{res}/t_{rec} [s]	Lower response toward	References
CuO NWs	365 nm 3 mW cm^{-2}	RT	–	100	–	–	[54]
ZnO/WO$_3^-$ NWs	365 nm 1.2 mW cm^{-2}	25	–	1000	–	–	[55]
SnO$_2$	313 nm 4 mW cm^{-2}	50	–	100	–	–	[56]
ZnO/GAC	365 nm 1 mW	RT	–	200	15/18	–	[57]
TiO$_2$/Pd NP	365 nm 2 mW cm^{-2}	33	–	–	45/24	C$_2$H$_4$O, C$_3$H$_6$O, C$_4$H$_8$O, NO, CO$_2$	[88]
PdO/WO$_3$	480 nm 150 mW cm^{-2}	RT	–	40	126/348	–	[89]
CeO$_2$/Pd/PDA/rGO	365 nm 0.89 mW cm^{-2}	100	15	6000	70/180	NH$_3$, CH$_4$. C$_3$H$_6$O, NO$_2$	[90]
SnO$_2$/Pd	365 nm 10 mW cm^{-2}	330	–	200	4/22,4	CH$_4$, C$_2$H$_6$, C$_2$H$_4$, C$_3$H$_8$, SO$_2$, C$_2$H$_5$OH	[92]
rGO/ZnO/Au	UV 2000 mW cm^{-2}	RT	–	500	8/612	NH$_3$, CH$_4$, C$_4$H$_{10}$, CO$_2$, O$_2$	[93]

electromagnetic wave with conductive, sub-wavelength NPs and its electrons induces a dipole moment inside the NP, while the curved shape of the NPs acts as a counter force against the driven electrons, allowing for resonance to arise.[99] These localized resonant oscillations of elections lead to the amplification of the electromagnetic field inside and in close proximity to the NP.[99] The absorbance and therefore optical extinction of light by the NP show a maximum at a certain wavelength, called the LSPR, and depend on the material, size, and shape of the NPs. Following Mie theory for spherical particles with radius much smaller than the incident wavelength, scattering of light increases drastically with particle size, which reduces LSPR efficiency.[98] The influence of nonspherical shapes on the plasmon resonance and gas sensitivity has been proven in experiments, though an analytical description is yet to be developed.[98,100] The wavelength for the plasmon resonance not only depends on the material, size, and shape of the NPs but also the refractive index of the surrounding medium, which is the basis for optical-sensing applications.[98]

During the non-radiative decay of surface plasmons, two kinds of energetic hot carriers are generated[101]: nonthermal hot carriers by Landau-like damping and thermalized hot carriers resulting from the relaxation process. These hot carriers are involved in various processes, such as the generation of secondary emissions, the amplification of chemical reactions, and the generation of electric current.[102,103] Nonthermal hot carriers are usually considered to be the main contributor for chemical conversions, still the less energetic thermal hot carriers participation cannot be excluded.[101] NPs of noble metals such as Au, Ag, and Pd are widely used for plasmonic-sensing applications through optical sensors, due to their large and tunable LSPR peaks, high stability, and biocompatibility.[104–106]

The integration of plasmonic NPs into semiconductor gas sensor designs has several advantages in addition to their photocatalytic activity. First, high surface to volume ratios of nanostructured materials lead to more active sites for hydrogen adsorption and consequently to a higher reactivity of the material.[107] Also, the LSPR of the plasmonic NPs can be precisely tuned to the vibrational frequency of hydrogen, resulting in a highly specific hydrogen sensor.[101,105] Finally, heterometallic sensor designs including plasmonic NPs enable for photonic activation of NPs with insufficient optical absorbance in certain wavelengths.[108] In recent years, various plasmonic NPs, including noble metal NPs (e.g., gold and silver), have been utilized in photocatalysis and chemical sensing,[109] but only a few focus on RT hydrogen detection on MOX gas sensors.[91,110–112] Therefore, we not only review recent developments in MOX gas sensors but also optical-sensing devices. To identify new materials and design opportunities for plasmonic MOX gas sensing, recent advances in photocatalytic hydrogen dissociation are also discussed in this section.

3.1. Photoactivated H$_2$ Dissociation by Plasmonic NPs and LSPR

A mechanism that proved to be effective for increasing the sensitivity and reaction times of MOX gas sensors to hydrogen is the previously mentioned spillover effect.[9] When hydrogen molecules adsorb on certain noble metal NPs, catalytic dissociation of molecules is followed by spillover of the atoms over the semiconductors' surface, increasing the probability of a reaction. Hydrogen can therefore more easily interact with the adsorbed oxygen on the MOX gas sensor surface and release electrons back into the semiconductor, increasing the conductivity.[9] Since plasmonic NPs can dissociate hydrogen molecules under illumination, these materials could allow for chemo-selective, photon-activated hydrogen sensing.[96] It has been shown that the LSPR of gold NPs can be tuned to the vibrational frequency of hydrogen gas, resulting in a highly specific and sensitive,

yet optical hydrogen sensor.[105] In this section, we will discuss recent developments in the field of light-activated H$_2$ dissociation on plasmonic NPs and LSPR at RT as a basis for light-activated H$_2$ gas sensing.

3.1.1. Hydrogen Dissociation on Noble Metal Plasmonic NPs

The first report of H$_2$ dissociation facilitated by plasmonic NPs at RT was submitted by Halas et al. where the formation of hydrogen deuteride (HD) from H$_2$ and D$_2$ was induced by hot electrons of Au plasmonic NPs of 5–30 nm immobilized on a TiO$_2$ support.[113] In 2013, their working group conducted similar experiments with SiO$_2$ as support material and were able to achieve an almost twofold increase in hydrogen conversion rate with linear dependence to light intensity.[114] They proposed that the Schottky barrier, formed between TiO$_2$ and gold NPs, might promote the transfer of hot electrons into the MOX support, reducing the number of available electrons for the hydrogen dissociation. A more detailed proposal of the mechanism was submitted by Yan et al. who examined the dynamics of hydrogen dissociation on a linear silver atomic chain via time-dependent density-functional theory.[106] Calculating the electron density around H$_2$ upon irradiation with femtosecond laser pulses, they predicted that hot electrons migrate to the antibonding state of hydrogen, inducing dissociation of the atoms. They also found that increasing the light intensity and chain length of Ag NPs also effectively raised the number of LSPRs and consequently the dissociation rate of hydrogen. However, Ag would be an interesting alternative to Au or Pd NPs due to its higher abundance, though long-term stability of the less noble catalyst would have an impact on the sensor's lifetime. Heterosystems of plasmonic noble metal NPs and the influence of different support materials were further tested by Collins et al.[115] Their working group investigated the hydrogen dissociation and migration of hydrogen atoms from Pt NPs to Au nanorods using TiO$_2$, ZnO, and SiO$_2$ as support materials. Interestingly, hydrogen did not migrate via spillover effect for silica supports but for both other tested MOXs. The authors therefore confirmed that this effect is indeed strongly dependent on the catalyst surface and only takes place on transition MOXs which could possibly allow for precise migration control of hydrogen even in very small areas.

3.1.2. Hydrogen Dissociation on Nonnoble Metal Plasmonic NPs

NPs made from nonnoble metals such as Mg, Al, In, Ga, and Ni also show plasmonic behavior.[95] Nonnoble metals are less stable than their noble metal counter parts, but could be used for cost efficient sensor designs due to their high abundance. Also, they absorb light in the UV rather than the visible light region,[95] which could be beneficial for light-enhanced recovery of MOX gas sensors.[116] Mg as new material for plasmonic applications in visible range was introduced by Sterl et al. in 2015.[117] They synthesized Mg nanodisks with diameters of ≈80, 160, and 220 nm with a thickness of ≈80 nm. Mg was protected against further oxidation by an intrinsic MgO passivation layer that formed on the nanodisks surface. With their experiments, they could prove that dissociation of hydrogen and hydrogenation of Mg to MgH$_2$ works at RT under irradiation in the visible range

and is reversible in oxygen atmospheres, though an influence of the MgO passivation layer cannot be excluded. Additionally, it was observed that hydrogenated Mg loses its plasmonic character, significantly changing the extinction spectra at the initial peak position. With the highly tunable response and the capacity to store up to 7.6 wt% hydrogen, Mg is an interesting material for hydrogen sensing with high saturation limits.[118] Also, the detection of adsorbed hydrogen via extinction or absorption spectra can easily be combined with chemoresistive gas sensors. It can be expected though that the formation of MgH$_2$, which has a very high formation enthalpy of roughly 76 kJ mol^{-1} and therefore usually requires elevated temperature or pressures, will be less efficient than the hydration of Pd.[119] Applying two different measuring principles, selectivity and accuracy of MOX gas sensors, could be significantly enhanced. Halas research group, who already demonstrated H$_2$ dissociation on Au NPs, could show that Al is also suitable for light-activated H$_2$ dissociation at RT.[120] Al nanocrystals with a diameter of 100 nm were synthesized by a wet-chemical approach and dispersed on an Al$_2$O$_3$ support. To exhibit the dissociation of hydrogen, again the generation of HD from H$_2$ and D$_2$ was measured with and without laser illumination at wavelengths between 300 and 1000 nm. They found two distinct absorption peaks associated with plasmonic resonance and the interband transition. Interestingly, the interband transition also yielded hot electrons, energetic enough to promote hydrogen dissociation, which is a unique feature of Al-based photocatalysts that opens up for more pathways of optically controlled hydrogen sensors and virtual sensor arrays. A heterometallic system of 20 wt% Cu NPs on a MgO/Al$_2$O$_3$ support was recently developed by the same working group.[101] The photocatalyst was synthesized by a coprecipitation method and showed instantaneous increase in HD formation and respectively H$_2$ dissociation when illuminated at 550 nm in the UV–vis range at 300 K. Investigating the dissociation rate as a function of light intensity, the authors suggested that for Cu plasmons, nonthermal HCs and their multiplication by electron–electron interactions are the driving forces of H$_2$ dissociation.

3.1.3. Plasmonic Antenna–Reactor Configurations

Another setup of plasmonic photocatalysts made from bimetallic systems proved to be applicable for H$_2$ dissociation by Zhang et al. in 2016.[121] Zhang et al. prepared Al–Pd nanodisk dimers via hole-mask colloidal lithography. As shown in **Figure 7**, the Al
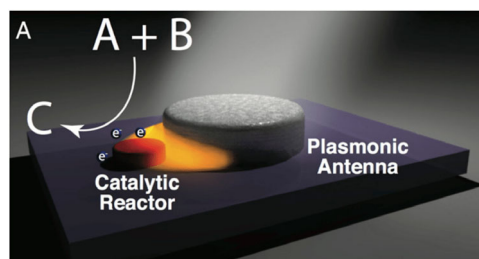
Figure 7. Schematic of the antenna–reactor mechanism with the plasmonic antenna (gray) receiving energy from the light source and focusing it on the catalytic reactor (red). Reproduced with permission.[108] Copyright 2016, PNAS.

disks served as plasmonic antennas that when illuminated with wavelengths of ≈500 nm induced a "forced plasmon" at the Pd surface. As a result, the photonically less absorbing Pd was also activated and acted as the reactor for the H_2 dissociation. Compared to pristine Pd nanodisks, the HD generation was increased by approximately sevenfold. Antenna–reactor configurations can be applied to other high selective metal catalysts that usually do not show sufficient absorbance for photoactivation.[108] Vadai et al. demonstrated that antenna–reactor configurations can also serve for the recovery of Pd-based hydrogen sensors and catalysts.[122] By coupling Pd nanocubes with Au nanodisks, the conversion of hydrogen-infused β-Pd to the α phase containing less than 3.5% hydrogen could be facilitated by illumination. Combined with laser desorption, this might be a very effective way of recovering catalysts and sensor materials. Still, both Zhang et al. and Vadai et al. emphasized the importance of the spatial arrangement of plasmonic antenna and catalytic reactor, as well as their distance. Imaging the dehydrogenation process in situ with scanning TEM and TEM, it could be observed that the enhanced electromagnetic fields induced by the plasmonic NPs are not located homogenously but have a higher abundance on Pd sites closer to the plasmon.[122] In their review article, Sytwu et al. noted that the distance of both catalysts should be kept as small as possible but not close enough for quantum effects like tunneling (<1 nm) or localization of surface charges to occur (<2–5 nm).[123] This again shows the importance of highly precise fabrication methods for the application of plasmonic NPs and especially this geometry in gas sensors. Still, it could also enable for highly site-selective photoactivated reactions, highly suitable for intelligent sensor designs.

3.2. Application of Plasmonic NPs in Hydrogen Gas Sensors

3.2.1. Chemoresistive MOX Hydrogen Sensors

The combination of plasmonic NPs and chemoresistive MOX gas sensors is a very promising attempt to enhance sensitivity and enable RT operation.[124] Even though plasmonic NPs have been used for enhanced optical sensing for over 30 years,[125] we found that the literature concerning plasmon-enhanced chemoresistive gas sensors is very limited. For example, Pd, a common plasmonic material, is widely used for enhanced sensing performance of MOX gas sensors, due to the high sensitivity and selectivity of hydride formation, but plasmonic effects are not often considered for new sensor designs.[126] Yet, some of the publications mentioned in Section 2.2 might also contribute to this list, but the plasmonic surface effects were not considered in those cases. To our knowledge, only about 20 publications deliberately utilize plasmonic NPs for MOX gas sensors[38,50,86,91,110,111,127–143] with a vast majority yet again focused on NO_2 detection.[38,111,128,129,131–133,138–143] For example, Kim et al. decorated commercially available ZnO NWs with Au NPs of 10 nm in a wet-chemical approach and transferred them on an interdigital electrode to observe the sensing performance.[131] They exhibited a three-fold increase in response toward 1 ppm NO_2, when illuminated with a green LED laser at 532 nm, compared to nondecorated ZnO NWs. Also, the response time of the sensor was lowered by 86%.

The improvement was mainly attributed to the generation of hot electrons but other catalytic and optical effects might also contribute. Wang et al. also investigated the selectivity of an equal system to NH_3 and NO_2.[38] ZnO nanorods of ≈15 nm were synthesized by a wet-chemical approach and subsequently functionalized with Au NPs via a photoreduction method. Under illumination with yet again 532 nm, the sensor showed a higher selectivity toward NO_2, whereas without illumination, the device was more selective toward NH_3. Altering the operation mode of such a light-controlled sensor might therefore further enhance the selectivity of Pd-based hydrogen sensors and well suitable for the application in sensor arrays to avoid elongated reaction times.

Despite the low abundance of literature, there are a few publications that target hydrogen as analyte.[91,110–112] Sturaro et al. synthesized ZnO nanocrystals by a heat-up colloidal method and doped them with different concentrations of Ga using a wet-chemical approach.[111] In their work, both the resistance and change in optical absorbance due to LSPR were considered as sensor signals, yet the measurements were done separately. For optical measurements, the nanocrystals were spin-coated on SiO_2 glass substrates and absorption was measured from 350 to 2000 nm with operating temperatures between 80 and 200 °C during contact with NO_2 and H_2. For electrical measurements the nanocrystals were coated on a Si/Si_3N_4 support and resistance was measured at 80 and 150 °C. Unfortunately, the sensor showed a higher selectivity toward NO_2 for both measurements, and only a neglectable change in resistance upon H_2 exposure could be observed even when operating at 150 °C. In a later study Pt NPs were added to the sensor design, to further increase sensor performance.[112] The optical response of the sensor toward hydrogen was significantly enhanced, though chemoresistive response to H_2 was still neglectable. The authors concluded that the chosen operating temperatures were insufficient and could not be compensated by illumination. Choosing a different semiconductor, Cattabiani et al. could achieve not only a more responsive but also rather slow sensor detecting hydrogen at RT.[110] SnO_2 NWs were grown with the vapor–liquid–solid method an Al_2O_3 substrates, precoated with Pt and subsequently functionalized with Ag NPs by radio frequency (RF) sputtering. Under irradiation with a green LED, the response of the sensor was increased by roughly 33%, but the light exposure did not have an influence on the long reaction times of few minutes. Yet again, the authors point out that both fields, MOX gas sensors loaded with metallic NPs and plasmon-driven catalysis, are strongly interconnected. As the most efficient example of plasmonic NP utilization for MOX hydrogen sensors, Kumar et al. developed a highly sensitive hydrogen sensor based on ZnO and Au thin films.[91] ZnO and subsequently Au were deposited on Al_2O_3 substrate via magnetron sputtering in RF mode. Performance tests were carried out under 50–1000 ppm hydrogen at an elevated operating temperature of 250 °C. At a concentration of 1000 ppm, the sensor response could be increased more than twofold under illumination with UV light at 365 nm. They could also show that their sensor exhibits selectivity toward hydrogen compared to other reducing gas species. For example, the response to 1000 ppm CH_4 was over three times smaller compared to hydrogen. Since all of the tested gas species still altered the resistance of the sensitive layer to some extent,

identification of the adsorbed gas species would still be impossible with just one sensor signal. The small range of semiconductive sensor materials and plasmonic NPs that have been tested in this context shows that a lot of research still has to be done.

3.2.2. Optical Plasmonic Hydrogen Sensors

In addition to MOX gas sensors relying on a change in resistance, optical gas sensors can also utilize plasmonic NPs for the detection of hydrogen, even in explosive atmospheres.[144] The optical detection of hydrogen via surface plasmons is not a new idea but was already shown by Chadwick and Gal in 1992.[125] They demonstrated that surface plasmons in Pd could serve for highly effective hydrogen sensing even at RT and enhanced optical-sensing performance. The same effect was later utilized by Langhammer et al. in 2007, where hydride formation due to hydrogen incorporation in Pd nanodisks significantly altered the intensity and peak position in the absorbance spectrum of the plasmonic material.[145] The shift in LSPR wavelength is proportional to the refractive index of the surrounding medium and can be used for analyte gas detection.[99,146] Since size, shape, and composition of plasmonic NPs play a significant role in determining their LSPR behavior,[120] various types of plasmonic NPs have been tested for optical hydrogen detection and proved to be effective at RTs.[105,125,147] Still, the synthesis and design of plasmonic NPs with specific optical and physical properties remain a major challenge.[96]

In recent publications, plasmonic MOXs of TiO_2,[148] WO_3,[149] and MoO_3[150] have even been combined with plasmonic noble metals for optical hydrogen detection. A full overview of the performance of optical and also chemoresistive gas sensors from the previous section is shown in **Table 2**. Gazzola et al. were able to show that TiO_2 in anatase deposited on gold monolayers by spin-coating can be used as a plasmonic hydrogen-sensing material.[148] When illuminated with wavelengths of 480–680 nm, a noticeable change in absorbance could be observed during hydrogen exposure. Yet their experiments were carried out at high temperatures of 300 °C with elevated hydrogen concentrations of 1%–5%, showing rather long recovery times of over 15 min. In contrast, a very responsive novel LSPR hydrogen sensor was reported by Mikami et al.[147] They developed an optical fiber sensor using commercially available Pd NPs of 4 nm, which were immobilized by poly-L-lysine and coated on a hetero-core fiber. Measuring the transmission with illumination of the sensor by an LED at 850 nm, they could achieve the fastest response and recovery times in this review of 1.5 and 3.2 s responding to 4% H_2 in N_2. LSPR sensors have a wide detection range from percentage to ppm[151,152] and most recently even ppb range.[153] Sterl et al. systematically studied design principles on Pd nanodisk arrays.[151] The sensors were prepared by evaporation of a 20 nm Pd layer on an Au mirror using MgF_2 as spacer. With their experiments, they showed that for reflective measurements of plasmonic optical sensors, the readout wavelength should be chosen not only based on the material but also the desired concentration range. Watkins in contrast produced anisotropic nanostructured Pd films by oblique angle deposition.[152] The porous film consisted of agglomerated Pd NPs of 10 nm size, separated by narrow gaps. Their results show fast response times of 3.5 s to 64% H_2 in air but those drastically increased to 185 s at the lowest measured concentration of 100 ppm. In the case of Pd-based hydrogen-sensing devices, it is known that irreversible poisoning effects due to different gases like sulfuric compounds or even carbon monoxide can hinder hydrogen dissociation on the catalyst.[154,155] Daramadi et al. were able to overcome this issue with ternary PdAuCu NP alloys combining the CO resistance of PdCu alloys with the higher sensing performance of PdAu alloys.[154] Applying this sensor design, high resistance against CO, CO_2, and CH_4 poisoning and fast response and recovery times of 0.4 and 5.0 s operating at only 30 °C could be achieved.

Table 2. Overview of optical and chemoresistive plasmonic hydrogen sensors and their performance parameters reviewed in this article, including the type of light source, operating temperature, and measured H_2 concentration range for each sensor.

Material	Light source	T [°C]	Range (H_2) [ppm]	References
Au NP on ZnO Nano (NS)	365 nm —	250	50–1000	–
Ag NP on SnO_2 NW	Green LED —	RT	500	[110]
Pt/Ga NP on ZnO nano crystals (NC)	430 nm 770 µW cm^{-2}	80–200	50–1000	[111,112]
Ga NP on ZnO NC	350–2500 nm	80–200	10 000	[111,112]
TiO_2 (anatase)	–	300	10 000	[146]
Pd Np on hetero-core fiber structure	850 nm	RT	40 000	[147]
Au NP on TiO_2 NC	610 nm	300	10 000–50 000	[148]
Pd/Pt/Au WO_3 composite films	900 nm	200–250	10 000	[149]
Pd–MoO_3 NP	190–1100 nm		5000–100 000	[150]
Pd NP	400–1000 nm	RT	5000–50 000	[151]
NS Pd	885 nm	22	2 ppm—100%	[152]
Periodic Pd NP	200–1000 nm	RT	0.25–1000	[153]
PdAuCu alloy	400–1000 nm	30	5 ppm—100%	[154]

This reaction time would be within the requirements of the DOE for the development of hydrogen safety sensors, though the tested concentration range of 0.25–1000 ppm is still far too low compared to the LEL.

Overall it can be concluded that both MOX gas sensors and optical sensors can be based on similar materials and can both detect hydrogen at RT, though with different measuring ranges and mechanisms for the sensor response. Still there is a lot of work to be done to fully investigate the sensor performance of the different approaches considering environmental effects like humidity, temperature changes, and reactivity toward different gases. Because of their simple and highly miniaturizable designs, both concepts could complement each other to create small and cost-effective devices for reliable hydrogen detection over a wider concentration range from ppm to percentages. The combination of different measuring principles might also increase the reliability of the sensor readout and enable for increased selectivity utilizing advanced data evaluation methods like machine-based learning.

4. Conclusion

To conclude this review article, our findings show that semiconductor gas sensors have improved significantly in the recent years with respect to operating temperatures, cross selectivities, and reaction times. Yet, none of the evaluated developments fulfill multiple goals set by the DOE for hydrogen safety sensors. Especially the operation below RT, sensitivity toward other reducing gases like ammonia and the low measuring range remain challenging. Nonetheless, the activation of semiconductor gas sensors with light under the right conditions and implementation of plasmonic NPs are versatile pathways that might enable for cheap, yet highly efficient and safe hydrogen detection tools, capable of operating near RT. Photonic activation not only increases the sensitivity of a sensor but can also enhance its response and recovery times. Another optimization method, that proved effective in increasing the sensitivity and also selectivity of an MOX gas sensor toward hydrogen, is the decoration of the sensor surface with noble metal particles, like Au, Ag, and most commonly Pd. Since noble metals vastly increase production costs of a sensor, their usage has to be viewed critically from an economical point of view. The efficiency of the expensive catalyst could be increased by photoactivation, though financial benefits would depend on the additional optical equipment needed. Only a small fraction of publications combines irradiation and noble metal decoration of MOX gas sensors, showing that there is still a lot of research to be done, considering different material compositions, irradiation conditions, and also environmental influences like humidity and temperature changes. As already mentioned, missing standardization is a key issue for sensor development and evaluation since inconsistent measuring parameters and definitions for performance indicators throughout the literature makes a comparison of data impracticable in many cases.

Both photoactivation of semiconductors and enhancement of sensor performance with metal NPs are commonly applied in research fields of photocatalysis and optical gas sensing. Plasmonic NPs might therefore combine both pathways and connect the different research disciplines, to generate a knowledge transfer from photocatalysis to semiconductive gas sensors. Since hydrogen dissociation is a key process for both hydrogen sensing and also catalytic reactions, materials studied for efficient photocatalytic dissociation might be integrated into MOX sensor designs. Investigating dissociation performance of less noble metal particles, Al and Mg could be identified as interesting cost-efficient materials for hydrogen sensing, though the degradation and therefore long-term stability of the sensitive layer has to be concerned. Additionally, plasmonic antenna configurations can enhance the LSPR on materials with insufficient optical absorption properties, vastly increasing the list of possible candidates for light-activated gas sensing. Since those configurations require high precision deposition of materials, their commercial use is highly dependent on the development of scalable and reproducible fabrication techniques.

Compared to chemoresistive gas sensors, a higher number of optical plasmonic hydrogen sensors were developed in recent years. We found that both sensor designs share equal materials and are both suitable for fast RT hydrogen detection, yet with higher concentrations of hydrogen measurable by optical devices. The combination of optical and electronic readout of the sensor might be an interesting attempt to cover a wider measuring range of semiconductor gas sensors and also ensure a more reliable hydrogen detection due to complementary signal evaluation methods. As selectivity remains one of the main challenges for both sensor types, the development of a multimodal measuring system that correlates both reaction mechanisms could aid in reducing these problems significantly.

Conflict of Interest

The authors declare no conflict of interest.

[1] K. Mazloomi, C. Gomes, *Renewable Sustainable Energy Rev.* **2012**, *16*, 3024.

[2] International Energy Agency (IEA), IE, Net Zero by 2050, IEA, Paris **2021** https://www.iea.org/reports/net-zero-by-2050, Licence: CC BY 4.0 (accessed: August 2024).

[3] U. Schmidtchen, in *Fuels-Safety: Hydrogen: Overview*, Elsevier, Amsterdam **2009**.

[4] S. Dorofeev, A. Kochurko, A. Efimenko, B. Chaivanov, *Nucl. Eng. Design* **1994**, *148*, 305.

[5] W. J. Buttner, M. B. Post, R. Burgess, C. Rivkin, *Int. J. Hydrogen Energy* **2011**, *36*, 2462.

[6] G. Heiland, *Z. Phys.* **1954**, *138*, 459.

[7] T. Seiyama, A. Kato, K. Fujiishi, M. Nagatani, *Anal. Chem.* **1962**, *34*, 1502.

[8] K. Grossmann, U. Weimar, N. Barsan, in *Oxide Semiconductors*, Vol. *88*, Elsevier, Amsterdam **2013**, p. 261.

[9] B. Sharma, A. Sharma, J.-S. Kim, *Sens. Actuators B: Chem.* **2018**, *262*, 758.

[10] M. V. Nikolic, V. Milovanovic, Z. Z. Vasiljevic, Z. Stamenkovic, *Sensors* **2020**, *20*, 6694.

[11] T. Li, W. Zeng, H. Long, Z. Wang, *Sens. Actuators B: Chem.* **2016**, *231*, 120.

[12] D. E. Williams, P. T. Moseley, *J. Mater. Chem.* **1991**, *1*, 809.

[13] N. Barsan, U. Weimar, *J. Electroceram.* **2001**, *7*, 143.

[14] Y. Shi, H. Xu, T. Liu, S. Zeb, Y. Nie, Y. Zhao, X. Qin, X. Jiang, *Mater. Adv.* **2021**, *2*, 1530.

[15] X. Wang, X. Yang, *Surf. Sci.* **2022**, *721*, 122064.

[16] M. R. Alenezi, A. S. Alshammari, K. D. G. I. Jayawardena, M. J. Beliatis, S. J. Henley, S. R. P. Silva, *J. Phys. Chem. C* **2013**, *117*, 17850.

[17] F. Odobel, L. Le Pleux, Y. Pellegrin, E. Blart, *Acc. Chem. Res.* **2010**, *43*, 1063.

[18] S. Ahmed, S. K. Sinha, *Environ. Sci. Pollut. Res. Int.* **2023**, *30*, 24975.

[19] S. Choopun, N. Hongsith, E. Wongrat, in *Nanowires - Recent Advances*, (Ed.: X. Peng), InTech **2012**.

[20] A. Živković, N. H. de Leeuw, *Phys. Rev. Mater.* **2020**, *4*, 074606.

[21] Y.-F. Sun, S.-B. Liu, F.-L. Meng, J.-Y. Liu, Z. Jin, L.-T. Kong, J.-H. Liu, *Sensors* **2012**, *12*, 2610.

[22] C. Xu, J. Tamaki, N. Miura, N. Yamazoe, *Sens. Actuators B: Chem.* **1991**, *3*, 147.

[23] Z. Hijazi, D. D. Caviglia, M. Valle, in *Smart Sensors for Environmental and Medical Applications* (Eds.: H. Hallil, H. Heidari), Wiley **2020**, p. 129.

[24] B. Saruhan, R. Lontio Fomekong, S. Nahirniak, *Front. Sens.* **2021**, *2*, 657931.

[25] M. S. Barbosa, P. H. Suman, J. J. Kim, H. L. Tuller, J. A. Varela, M. O. Orlandi, *Sens. Actuators B: Chem.* **2017**, *239*, 253.

[26] H. Kwon, Y. Lee, S. Hwang, J. K. Kim, *Sens. Actuators B: Chem.* **2017**, *241*, 985.

[27] S. Lu, Y. Zhang, J. Liu, H.-Y. Li, Z. Hu, X. Luo, N. Gao, B. Zhang, J. Jiang, A. Zhong, J. Luo, H. Liu, *Sens. Actuators B: Chem.* **2021**, *345*, 130334.

[28] T. van Nguyen, V. C. Nguyen, D. van Nguyen, S. H. Hoang, N. Hugo, D. H. Nguyen, H. van Nguyen, *J. Hazard. Mater.* **2016**, *301*, 433.

[29] D. Jung, M. Han, G. S. Lee, *ACS Appl. Mater. Interfaces* **2015**, *7*, 3050.

[30] M. Reddeppa, B.-G. Park, M.-D. Kim, K. R. Peta, N. D. Chinh, D. Kim, S.-G. Kim, G. Murali, *Sens. Actuators B: Chem.* **2018**, *264*, 353.

[31] S. Z. N. Demon, A. I. Kamisan, N. Abdullah, S. A. M. Noor, O. K. Khism, N. A. M. Kasim, M. Z. A. Yahya, N. A. A. Manaf, A. F. M. Azmi, N. A. Halim, *Sens. Mater.* **2020**, *32*, 759.

[32] S. Yang, Z. Wang, Y. Hu, X. Luo, J. Lei, D. Zhou, L. Fei, Y. Wang, H. Gu, *ACS Appl Mater Interfaces.* **2015**, *7*, 9247.

[33] D. Sett, D. Basak, *Sens. Actuators B: Chem.* **2017**, *243*, 475.

[34] M. Tonezzer, *Sens. Actuators B: Chem.* **2019**, *288*, 53.

[35] D. E. Motaung, G. H. Mhlongo, P. R. Makgwane, B. P. Dhonge, F. R. Cummings, H. C. Swart, S. S. Ray, *Sens. Actuators B: Chem.* **2018**, *254*, 984.

[36] W. Ding, N. Ansari, Y. Yang, K. Bachagha, *Int. J. Hydrogen Energy* **2021**, *46*, 28823.

[37] J. D. Prades, R. Jimenez-Diaz, F. Hernandez-Ramirez, S. Barth, A. Cirera, A. Romano-Rodriguez, S. Mathur, J. R. Morante, *Sens. Actuators B: Chem.* **2009**, *140*, 337.

[38] J. Wang, S. Fan, Y. Xia, C. Yang, S. Komarneni, *J. Hazard. Mater.* **2020**, *381*, 120919.

[39] J. Wang, H. Shen, Y. Xia, S. Komarneni, *Ceram. Int.* **2021**, *47*, 7353.

[40] S. Mishra, C. Ghanshyam, N. Ram, R. P. Bajpai, R. K. Bedi, *Sens. Actuators B: Chem.* **2004**, *97*, 387.

[41] D. E. Williams, G. S. Henshaw, K. F. E. Pratt, R. Peat, *J. Chem. Soc. Faraday Trans.* **1995**, *91*, 4299.

[42] G. Sakai, N. Matsunaga, K. Shimanoe, N. Yamazoe, *Sens. Actuators B: Chem.* **2001**, *80*, 125.

[43] J. Saura, *Sens. Actuators B: Chem.* **1994**, *17*, 211.

[44] M. Bodzek, M. Rajca, *Ecol. Chem. Eng. S* **2012**, *19*, 489.

[45] R. Kumar, X. Liu, J. Zhang, M. Kumar, *Nano-Micro Lett.* **2020**, *12*, 164.

[46] D. O. Scanlon, C. W. Dunnill, J. Buckeridge, S. A. Shevlin, A. J. Logsdail, S. M. Woodley, C. R. A. Catlow, M. J. Powell, R. G. Palgrave, I. P. Parkin, G. W. Watson, T. W. Keal, P. Sherwood, A. Walsh, A. A. Sokol, *Nat. Mater.* **2013**, *12*, 798.

[47] S.-W. Fan, A. K. Srivastava, V. P. Dravid, *Appl. Phys. Lett.* **2009**, *95*, 142106.

[48] M. Hayyan, M. A. Hashim, I. M. AlNashef, *Chem. Rev.* **2016**, *116*, 3029.

[49] M. Reddeppa, B.-G. Park, G. Murali, S. H. Choi, N. D. Chinh, D. Kim, W. Yang, M.-D. Kim, *Sens. Actuators B: Chem.* **2020**, *308*, 127700.

[50] F. Xu, H.-F. Lv, S.-Y. Wu, H.-P. Ho, *Sens. Actuators B: Chem.* **2018**, *259*, 709.

[51] G. Njio, T. Wagner, in *Proc. IMCS 2018*, AMA Service GmbH, Wunstorf **2018**, p. 905.

[52] Qomaruddin, O. Casals, A. Šutka, T. Granz, A. Waag, H. S. Wasisto, J. Daniel Prades, C. Fàbrega, *Sensors* **2020**, *20*, 850.

[53] B. Zhang, N. Bao, T. Wang, Y. Xu, Y. Dong, Y. Ni, P. Yu, Q. Wei, J. Wang, L. Guo, Y. Xia, *J. Alloys Compd.* **2021**, *867*, 159076.

[54] N. Sihar, T. Y. Tiong, C. F. Dee, P. C. Ooi, A. A. Hamzah, M. A. Mohamed, B. Y. Majlis, *Nanoscale Res. Lett.* **2018**, *13*, 150.

[55] S. Park, T. Hong, J. Jung, C. Lee, *Curr. Appl. Phys.* **2014**, *14*, 1171.

[56] T. Li, W. Zeng, D. Shi, S. Hussain, *Mater. Lett.* **2015**, *161*, 648.

[57] A. Saravanan, B.-R. Huang, D. Kathiravan, A. Prasannan, *ACS Appl. Mater. Interfaces* **2017**, *9*, 39771.

[58] A. Chizhov, M. Rumyantseva, A. Gaskov, *Nanomaterials* **2021**, *11*, 892.

[59] V. S. Bhati, M. Hojamberdiev, M. Kumar, *Energy Rep.* **2020**, *6*, 46.

[60] M. Kashif, M. E. Ali, S. M. U. Ali, U. Hashim, *Ceram. Int.* **2013**, *39*, 6461.

[61] Y. Shen, T. Yamazaki, Z. Liu, D. Meng, T. Kikuta, N. Nakatani, M. Saito, M. Mori, *Sens. Actuators B: Chem.* **2009**, *135*, 524.

[62] S. Öztürk, A. Kösemen, Z. A. Kösemen, N. Kılınç, Z. Z. Öztürk, M. Penza, *Sens. Actuators B: Chem.* **2016**, *222*, 280.

[63] Y. Tang, Y. Zhao, H. Liu, *ACS Sens.* **2022**, *7*, 3582.

[64] F. Xie, W. Li, Q. Zhang, S. Zhang, *IEEE Sens. J.* **2019**, *19*, 10674.

[65] H.-D. Dong, J.-P. Zhao, M.-X. Peng, Y.-H. Zhang, P.-Y. Xu, *Vacuum* **2023**, *207*, 111597.

[66] S. Agarwal, S. Kumar, H. Agrawal, M. G. Moinuddin, M. Kumar, S. K. Sharma, K. Awasthi, *Sens. Actuators B: Chem.* **2021**, *346*, 130510.

[67] K. Hassan, G.-S. Chung, *Sens. Actuators B: Chem.* **2017**, *239*, 824.

[68] Z. S. Hosseini, A. Mortezaali, A. Irajizad, S. Fardindoost, *J. Alloys Compd.* **2015**, *628*, 222.

[69] C. M. Aldao, in *Tin Oxide Materials*, Elsevier, Amsterdam **2020**, p. 101.

[70] M. Kumar, V. S. Bhati, M. Kumar, *Int. J. Hydrogen Energy* **2017**, *42*, 22082.

[71] K. Shun, K. Mori, S. Masuda, N. Hashimoto, Y. Hinuma, H. Kobayashi, H. Yamashita, *Chem. Sci.* **2022**, *13*, 8137.

[72] H. Shen, H. Li, Z. Yang, C. Li, *Green Energy Environ.* **2022**, *7*, 1161.

[73] K. D. Schierbaum, U. K. Kirner, J. F. Geiger, W. Göpel, *Sens. Actuators B: Chem.* **1991**, *4*, 87.

[74] P. Albers, J. Pietsch, S. F. Parker, *J. Mol. Catal. A: Chem.* **2001**, *173*, 275.

[75] J. Wang, C. Hu, Y. Xia, S. Komarneni, *Ceram. Int.* **2020**, *46*, 8462.

[76] Y. Liu, T. Shi, Q. Si, T. Liu, *Phys. Lett. A* **2021**, *391*, 127117.

[77] T. Hyodo, K. Urata, K. Kamada, T. Ueda, Y. Shimizu, *Sens. Actuators B: Chem.* **2017**, *253*, 630.

[78] F. H. Saboor, T. Ueda, K. Kamada, T. Hyodo, Y. Mortazavi, A. A. Khodadadi, Y. Shimizu, *Sens. Actuators B: Chem.* **2016**, *223*, 429.

[79] Y. Mun, S. Park, S. An, C. Lee, H. W. Kim, *Ceram. Int.* **2013**, *39*, 8615.

[80] A. Gaiardo, B. Fabbri, A. Giberti, V. Guidi, P. Bellutti, C. Malagù, M. Valt, G. Pepponi, S. Gherardi, G. Zonta, A. Martucci, M. Sturaro, N. Landini, *Sens. Actuators B: Chem.* **2016**, *237*, 1085.

[81] L. Giancaterini, S. M. Emamjomeh, A. de Marcellis, E. Palange, A. Resmini, U. Anselmi-Tamburini, C. Cantalini, *Sens. Actuators B: Chem.* **2016**, *229*, 387.

[82] T. Xie, N. Sullivan, K. Steffens, B. Wen, G. Liu, R. Debnath, A. Davydov, R. Gomez, A. Motayed, *J. Alloys Compd.* **2015**, *653*, 255.

[83] M. Šetka, M. Claros, O. Chmela, S. Vallejos, *J. Mater. Chem. C* **2021**, *9*, 16804.

[84] D. V. Ponnuvelu, B. Pullithadathil, A. K. Prasad, S. Dhara, K. Mohamed, A. K. Tyagi, B. Raj, *J. Mater. Sci.* **2017**, *28*, 9738.

[85] Q. Zhang, Z. Pang, W. Hu, J. Li, Y. Liu, Y. Liu, F. Yu, C. Zhang, M. Xu, *Appl. Surf. Sci.* **2021**, *541*, 148418.

[86] Y. Zhou, C. Zou, X. Lin, Y. Guo, *Appl. Phys. Lett.* **2018**, *113*, 82103.

[87] J. Noh, S.-H. Kwon, S. Park, K.-K. Kim, Y.-J. Yoon, *Sensors* **2021**, *21*, 1826.

[88] E. K. Alenezy, Y. M. Sabri, A. E. Kandjani, D. Korcoban, S. S. A. A. H. Rashid, S. J. Ippolito, S. K. Bhargava, *ACS Sens.* **2020**, *5*, 3902.

[89] X. Geng, Y. Luo, B. Zheng, C. Zhang, *Int. J. Hydrogen Energy* **2017**, *42*, 6425.

[90] H. Hashtroudi, A. Yu, S. Juodkazis, M. Shafiei, *Nanomaterials* **2022**, *12*, 1628.

[91] G. Kumar, X. Li, Y. Du, Y. Geng, X. Hong, *J. Alloys Compd.* **2019**, *798*, 467.

[92] P. Duan, H. Xiao, Z. Wang, Q. Peng, K. Jin, J. Sun, *Sens. Actuators B: Chem.* **2021**, *346*, 130557.

[93] Q. A. Drmosh, A. H. Hendi, M. K. Hossain, Z. H. Yamani, R. A. Moqbel, A. Hezam, M. A. Gondal, *Sens. Actuators B: Chem.* **2019**, *290*, 666.

[94] D. Li, J. Lu, X. Zhang, X. Peng, J. Li, Y. Yang, B. Hong, X. Wang, D. Jin, H. Jin, *J. Phys. Chem. C* **2022**, *126*, 14470.

[95] S. Kim, J.-M. Kim, J.-E. Park, J.-M. Nam, *Adv. Mater.* **2018**, *30*, e1704528.

[96] S. Li, P. Miao, Y. Zhang, J. Wu, B. Zhang, Y. Du, X. Han, J. Sun, P. Xu, *Adv. Mater.* **2021**, *33*, e2000086.

[97] M. J. Kale, T. Avanesian, P. Christopher, *ACS Catal.* **2014**, *4*, 116.

[98] K. M. Mayer, J. H. Hafner, *Chem. Rev.* **2011**, *111*, 3828.

[99] S. A. Maier, in *Plasmonics: Fundamentals and Applications*, Springer, New York **2007**.

[100] J. J. Mock, M. Barbic, D. R. Smith, D. A. Schultz, S. Schultz, *J. Chem. Phys.* **2002**, *116*, 6755.

[101] L. Zhou, M. Lou, J. L. Bao, C. Zhang, J. G. Liu, J. M. P. Martirez, S. Tian, L. Yuan, D. F. Swearer, H. Robatjazi, E. A. Carter, P. Nordlander, N. J. Halas, *Proc. Natl. Acad. Sci. U.S.A.* **2021**, *118*, e2022109118.

[102] A. Manjavacas, J. G. Liu, V. Kulkarni, P. Nordlander, *ACS Nano* **2014**, *8*, 7630.

[103] M. L. Brongersma, N. J. Halas, P. Nordlander, *Nat. Nanotechnol.* **2015**, *10*, 25.

[104] M. Guglielmi, A. Martucci, *J. Sol-Gel Sci. Technol.* **2018**, *88*, 551.

[105] D. Sil, K. D. Gilroy, A. Niaux, A. Boulesbaa, S. Neretina, E. Borguet, *ACS Nano* **2014**, *8*, 7755.

[106] L. Yan, Z. Ding, P. Song, F. Wang, S. Meng, *Appl. Phys. Lett.* **2015**, *107*, 83102.

[107] G.-J. Li, S. Kawi, *Mater. Lett.* **1998**, *34*, 99.

[108] D. F. Swearer, H. Zhao, L. Zhou, C. Zhang, H. Robatjazi, J. M. P. Martirez, C. M. Krauter, S. Yazdi, M. J. McClain, E. Ringe, E. A. Carter, P. Nordlander, N. J. Halas, *Proc. Natl. Acad. Sci. U.S.A.* **2016**, *113*, 8916.

[109] M. J. McClain, A. E. Schlather, E. Ringe, N. S. King, L. Liu, A. Manjavacas, M. W. Knight, I. Kumar, K. H. Whitmire, H. O. Everitt, P. Nordlander, N. J. Halas, *Nano Lett.* **2015**, *15*, 2751.

[110] N. Cattabiani, C. Baratto, D. Zappa, E. Comini, M. Donarelli, M. Ferroni, A. Ponzoni, G. Faglia, *J. Phys. Chem. C* **2018**, *122*, 5026.

[111] M. Sturaro, E. Della Gaspera, N. Michieli, C. Cantalini, S. M. Emamjomeh, M. Guglielmi, A. Martucci, *ACS Appl. Mater. Interfaces* **2016**, *8*, 30440.

[112] M. Rigon, V. Paolucci, M. Sturaro, S. M. Emamjomeh, C. Cantalini, A. Martucci, *Eurosensors* **2018**, *2*, 997.

[113] S. Mukherjee, F. Libisch, N. Large, O. Neumann, L. V. Brown, J. Cheng, J. B. Lassiter, E. A. Carter, P. Nordlander, N. J. Halas, *Nano Lett.* **2013**, *13*, 240.

[114] S. Mukherjee, L. Zhou, A. M. Goodman, N. Large, C. Ayala-Orozco, Y. Zhang, P. Nordlander, N. J. Halas, *J. Am. Chem. Soc.* **2014**, *136*, 64.

[115] S. S. E. Collins, M. Cittadini, C. Pecharromán, A. Martucci, P. Mulvaney, *ACS Nano* **2015**, *9*, 7846.

[116] D. Zhang, Z. Liu, C. Li, T. Tang, X. Liu, S. Han, B. Lei, C. Zhou, *Nano Lett.* **2004**, *4*, 1241.

[117] F. Sterl, N. Strohfeldt, R. Walter, R. Griessen, A. Tittl, H. Giessen, *Nano Lett.* **2015**, *15*, 7949.

[118] A. Zaluska, L. Zaluski, J. O. Strom–Olsen, *J. Alloys Compd.* **1999**, *288*, 217.

[119] M. Pozzo, D. Alfè, *Phys. Rev. B* **2008**, *77*, 104103.

[120] L. Zhou, C. Zhang, M. J. McClain, A. Manjavacas, C. M. Krauter, S. Tian, F. Berg, H. O. Everitt, E. A. Carter, P. Nordlander, N. J. Halas, *Nano Lett.* **2016**, *16*, 1478.

[121] C. Zhang, H. Zhao, L. Zhou, A. E. Schlather, L. Dong, M. J. McClain, D. F. Swearer, P. Nordlander, N. J. Halas, *Nano Lett.* **2016**, *16*, 6677.

[122] M. Vadai, D. K. Angell, F. Hayee, K. Sytwu, J. A. Dionne, *Nat. Commun.* **2018**, *9*, 4658.

[123] K. Sytwu, M. Vadai, J. A. Dionne, *Adv. Phys.: X* **2019**, *4*, 1619480.

[124] J. M. Suh, T. H. Eom, S. H. Cho, T. Kim, H. W. Jang, *Mater. Adv.* **2021**, *2*, 827.

[125] B. Chadwick, M. Gal, *Appl. Surf. Sci.* **1993**, *68*, 135.

[126] O. Lupan, V. Postica, F. Labat, I. Ciofini, T. Pauporté, R. Adelung, *Sens. Actuators B: Chem.* **2018**, *254*, 1259.

[127] N. Bhardwaj, S. Mohapatra, *Ceram. Int.* **2016**, *42*, 17237.

[128] C. Chen, Q. Zhang, G. Xie, M. Yao, H. Pan, H. Du, H. Tai, X. Du, Y. Su, *Mater. Res. Express* **2020**, *7*, 15924.

[129] T. A. T. Do, T. G. Ho, T. H. Bui, Q. N. Pham, H. T. Giang, T. T. Do, D. van Nguyen, D. L. Tran, *Beilstein J. Nanotechnol.* **2018**, *9*, 771.

[130] C. Han, X. Li, J. Liu, H. Dong, W. Cheng, Y. Liu, J. Xin, X. Li, C. Shao, Y. Liu, *Sens. Actuators B: Chem.* **2022**, *371*, 132448.

[131] D. W. Kim, K. H. Park, S.-H. Lee, C. Fàbrega, J. D. Prades, J.-W. Jang, *J. Colloid Interface Sci.* **2021**, *582*, 658.

[132] S.-H. Kwon, T.-H. Kim, S.-M. Kim, S. Oh, K.-K. Kim, *Nanoscale* **2021**, *13*, 12177.

[133] P. Chakrabarty, M. Banik, N. Gogurla, S. Santra, S. K. Ray, R. Mukherjee, *ACS Omega* **2019**, *4*, 12071.

[134] S.-B. Wang, Y.-F. Huang, S. Chattopadhyay, S. Jinn Chang, R.-S. Chen, C.-W. Chong, M.-S. Hu, L.-C. Chen, K.-H. Chen, *NPG Asia Mater.* **2013**, *5*, e49.

[135] Z. Q. Zheng, B. Wang, J. D. Yao, G. W. Yang, *J. Mater. Chem. C* **2015**, *3*, 7067.

[136] F. Zhou, Q. Wang, W. Liu, *Mater. Res. Express* **2016**, *3*, 85006.

[137] M. Karmaoui, L. Lajaunie, D. M. Tobaldi, G. Leonardi, C. Benbayer, R. Arenal, J. A. Labrincha, G. Neri, *Appl. Catal. B: Environ.* **2017**, *218*, 370.

[138] Qomaruddin, O. Casals, H. S. Wasisto, A. Waag, J. D. Prades, C. Fàbrega, *Chemosensors* **2022**, *10*, 28.

[139] S. Park, S. An, H. Ko, S. Lee, C. Lee, *Sens. Actuators B: Chem.* **2013**, *188*, 1270.

[140] C. Yao, L. Wu, H. Li, N. Xu, J. Sun, J. Wu, *Appl. Surf. Sci.* **2022**, *584*, 152508.

[141] B. Zhang, S. Zhang, Y. Xia, P. Yu, Y. Xu, Y. Dong, Q. Wei, J. Wang, *Nanomaterials* **2022**, *12*, 4062.

[142] J. Hu, X. Liu, J. Zhang, X. Gu, Y. Zhang, *Sens. Actuators B: Chem.* **2023**, *382*, 133505.

[143] K. Lee, I. Cho, M. Kang, J. Jeong, M. Choi, K. Y. Woo, K.-J. Yoon, Y.-H. Cho, I. Park, *ACS Nano* **2023**, *17*, 539.

[144] A. Tittl, P. Mai, R. Taubert, D. Dregely, N. Liu, H. Giessen, *Nano Lett.* **2011**, *11*, 4366.

[145] C. Langhammer, I. Zorić, B. Kasemo, B. M. Clemens, *Nano Lett.* **2007**, *7*, 3122.

[146] E. Gazzola, M. Cittadini, L. Brigo, G. Brusatin, M. Guglielmi, F. Romanato, A. Martucci, in *Plasmonics: Metallic Nanostructures and Their Optical Properties XIII* (Eds.: A. D. Boardman, D. P. Tsai), SPIE August **2015**, p. 95471D.

[147] M. Mikami, D. Komatsu, A. Hosoki, M. Nishiyama, H. Igawa, A. Seki, S. Kubodera, K. Watanabe, *Opt. Express* **2021**, *29*, 48.

[148] E. Gazzola, M. Cittadini, M. Angiola, L. Brigo, M. Guglielmi, F. Romanato, A. Martucci, *Nanomaterials* **2020**, *10*, 1490.

[149] M. Ando, R. Chabicovsky, M. Haruta, *Sens. Actuators B: Chem.* **2001**, *76*, 13.

[150] A. R. Shafieyan, M. Ranjbar, P. Kameli, *Int. J. Hydrogen Energy* **2019**, *44*, 18628.

[151] F. Sterl, N. Strohfeldt, S. Both, E. Herkert, T. Weiss, H. Giessen, *ACS Sens.* **2020**, *5*, 917.

[152] W. L. Watkins, Y. Borensztein, *Sens. Actuators B: Chem.* **2018**, *273*, 527.

[153] F. A. A. Nugroho, P. Bai, I. Darmadi, G. W. Castellanos, J. Fritzsche, C. Langhammer, J. Gómez Rivas, A. Baldi, *Nat. Commun.* **2022**, *13*, 5737.

[154] I. Darmadi, F. A. A. Nugroho, S. Kadkhodazadeh, J. B. Wagner, C. Langhammer, *ACS Sens.* **2019**, *4*, 1424.

[155] T. Hübert, L. Boon-Brett, G. Black, U. Banach, *Sens. Actuators B: Chem.* **2011**, *157*, 329.

Ingo Weyrauch holds an M.Sc. degree in analytical chemistry and quality insurance from the University of Applied Science Bonn-Rhein-Sieg and is currently pursuing a Ph.D. degree under the supervision of Prof. Peter Kaul at the Institute of Safety Research (ISF) and Member of the Graduate School for Applied Research in North Rhine-Westphalia (PK NRW). He works as a research associate at the German Aerospace Center (DLR) institute for the Protection of Terrestrial Infrastructures. His research focuses on gas sensing, particularly in the field of hydrogen, and the development of sensitive coatings.

Eva Louisa Hefler holds an M.Sc. degree in mechanical and industrial engineering from the University of Applied Sciences Köln and is currently pursuing a Ph.D. degree at the University of Wuppertal in the field of drone defense modeling. She is a research associate at the German Aerospace Center (DLR), where her work has focused on the optimization of semiconductor gas sensors using laser techniques in the field of laser physics.

Rene Breuch earned his M.Sc. degree in chemistry from the University of Wuppertal, Germany. He is currently pursuing a Ph.D. at the University of Applied Science Bonn-Rhein-Sieg and the University of Siegen, under the supervision of Prof. P. Kaul at the Institute for Safety and Security Research (ISF) in Rheinbach, Germany. Additionally, he works as a researcher at the German Aerospace Center (DLR), within the Institute for the Protection of Terrestrial Infrastructures. His research interests include nanomaterials, gas sensors, and Raman spectroscopy for various applications.

Peter Kaul studied physics at TU Braunschweig and RWTH Aachen, earning his Diploma in 1992. While working at SICAN Group Hannover, he completed his Ph.D. at the University of Gießen, receiving his doctorate in 1996. Since 1998, he has been a professor of physics, statistics, and measuring techniques at Bonn-Rhine-Sieg University of Applied Sciences. For more than 20 years, he has been working in the fields of sensor technology, microsensors, chemical sensors for gases and liquids, signature propagation of explosive traces, biosensors, signal processing, multi-sensor systems, as well as detection methods for explosives and odor components.

Sanjay Mathur is Director and Chair of the Institute of Inorganic and Materials Chemistry at University of Cologne, Germany. He is an Academician of the World Academy of Ceramics and served as the President of the American Ceramic Society (ACerS, 2022-23). He is a Fellow of the American Ceramics Society, ASM International and Materials Research Society, and he earned his DPhil degree (1992) at the Chemical Laboratories, University of Rajasthan, Jaipur, India, and his Habilitation degree (2004) at the Saarland University, Germany. His research interests include chemical processing of functional inorganic materials for batteries, sensors, and green hydrogen production, as well as in the development of bioconjugated nanoparticles for tracking intracellular processes. He has published >550 articles (h index, 78) and edited/written several books/book chapters, and holds 11 patents.

Kostyantin Konstantynovski is the Head of the "Detection Systems" Department at the German Aerospace Center, specializing in the development and application of technologies for detecting hazardous substances, particularly in the CBRNE domain (chemical, biological, radiological, nuclear, and explosive materials). With a background in chemistry and a doctorate from the University of Cologne, he has extensive experience in R&D of advanced sensor and detection systems. He has also worked as a research associate and lecturer at the Bonn-Rhein-Sieg University of Applied Sciences and is currently active as an expert for the European Commission on a part-time basis.